EFFECTS OF PARTICLE SIZE DISTRIBUTION ON SURFACE FINISH OF SELECTIVE LASER MELTING PARTS

J H Lim[1], N A Khan[1]

[1] Advanced Remanufacturing and Technology Centre, 3 Cleantech Loop, Singapore 637143

Abstract

Metal parts produced by Selective Laser Melting (SLM) usually exhibit poor surface finish compared to conventional manufacturing processes. There is a growing need for parts to have good surface quality in the as-built condition to minimise post-processing costs and reduce lead time. There are many studies done on the effects of processing parameters on surface finish but very little on the influence of powder characteristics. This study aims to investigate the effects of Particle Size Distribution (PSD) on surface finish of AM parts by printing coupons with Inconel 625 powders of varying PSD. It was found that roughness of internal surfaces was mainly caused by the presence of partially sintered particles. Whilst a smaller particle mean size and wider particle size range are preferred for better surface finish, a powder that is too fine may result in poor flowability affecting its processability in terms of layering and powder bed quality.

Introduction

Laser Powder Bed Fusion (L-PBF) is an Additive Manufacturing (AM) process in which powder materials fuse together layer by layer to form a three dimensional (3D) part based on a computer aided design (CAD) model [1]. For fabrication of metal components, this process is often referred to as Selective Laser Melting (SLM) or Direct Metal Laser Sintering (DMLS). During the fabrication process, a thin layer of metal powder material is deposited onto a build platform with a roller or coater blade. A focused laser beam scans the powder bed based on the cross-section of the three dimensional CAD model to selectively fuse the layer of powder. The build platform is then lowered by a fixed layer thickness before a new layer of powder is being deposited on the powder bed. The laser beam scans the powder bed again and the process of joining materials layer by layer repeats itself until the whole three dimensional part is produced.

It is widely known that AM is capable of producing highly complex parts with faster processing time [2]. However, parts produced by L-PBF usually exhibit poor surface finish compared to conventional manufacturing processes. Post-processing techniques, such as shot peening, machining and polishing, are often required to achieve desired surface finish [3]. These post-processes can be costly and challenging especially for parts with small or intricate internal features such as conformal cooling channels used for tooling. For AM to reach a state of maturity for industrial applications, there is a growing need for parts to have good surface quality in the as-built condition to minimise post-processing cost and reduce lead time [4].

Surface quality of as-built part is dependent not only on part geometry and process parameters [8-10] but can also be influenced by feedstock powder characteristics such as particle size distribution (PSD) [5-7]. PSD refers to the amount of large and small particles in the powder. Energy supplied by the laser may be insufficient to fully melt the large particles and the partially melted particles may result in surface undulation causing an increase in surface roughness.

However, if sufficient small particles are present, it may help to reduce this effect as small particles can fill into the voids between large particles and are easily melted. Hence, a powder with lower particle mean size and wider particle size range tend to produce parts with better surface finish.

Surface quality can also be affected by the effective layer thickness (t_{eff}) [11-13], which is the actual powder layer thickness deposited on the part after each scanned layer and is always higher than the theoretical layer thickness (t_0). For metal powders used in SLM, the powder layer density typically lies between 40% to 60%. Assuming that the first layer of powder is deposited at a layer thickness of 30µm and has a powder layer density of 60%, the laser scans that layer to a bulk density of 99%. This leads to a shrinkage in bulk layer thickness to approximately 18.2µm, a difference of 11.8µm. The build platform then lowers by the theoretical layer thickness of 30µm for the next layer of powder to be deposited. This results in an effective layer thickness of 41.8µm as illustrated in Figure 1.

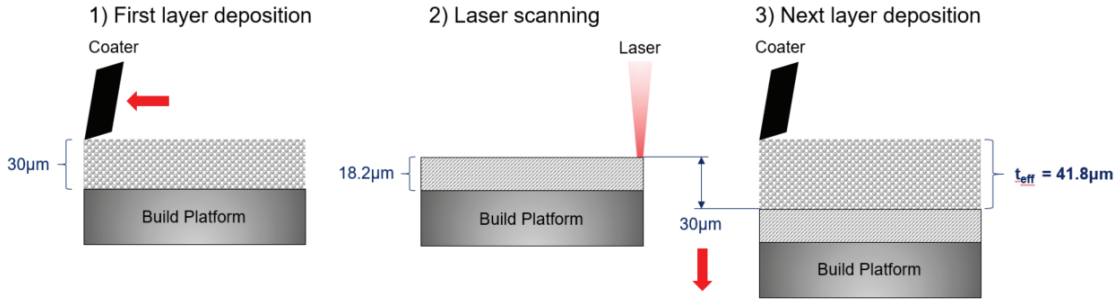

Figure 1: Development of effective layer thickness in SLM

Assuming a constant mass before and after laser scanning and the shrinkage occurs in the Z-direction, t_{eff} can be calculated based on the powder layer density and part density using the following equations. Note that $t_{eff(0)} = t_0$ since it represents the first layer of powder deposition.

$$t_{part(i)} = \frac{Packing\ Density * t_{eff(i-1)}}{Part\ Density} \quad (1)$$

$$t_{eff(i)} = \left[t_{eff(i-1)} - t_{part(i)} \right] + t_0 \quad (2)$$

where t_{part} = layer thickness of bulk layer
t_{eff} = effective layer thickness
t_0 = theoretical layer thickness
i = layer number

More importantly, t_{eff} has to be considered in relation to the particle size when understanding the effects on surface quality. For example, if t_{eff} < D90 of the powder, particles that are larger than t_{eff} will not be deposited in the powder layer as they will be pushed across the build surface by the coater blade. The effect of large particles will be less significant and the presence of small particles will have a greater effect in improving surface finish. However, if t_{eff} > D90, large particles can be deposited in the powder layer so surface roughness will be attributed to the size and quantity of the large particles present. The effect of small particles

become less significant in improving surface finish. This means that the higher the effective layer thickness, the greater the influence of large particles and the lower the influence of small particles on surface finish.

Although it has been suggested the use of fine particles for better surface finish [11-13], most studies are limited to external surfaces of simple geometries i.e. top and side surfaces of cubes and walls. The study on the influence of powder characteristics on surface quality of internal surfaces would be of greater interest and importance because these surfaces are hard to reach and more challenging to post-process. This study aims to investigate the effects of PSD on surface finish of internal channels comprising of inclined and overhanging surfaces.

Methods and Materials

Gas atomised IN625 powders of three different PSDs were requested from the same production batch with specifications shown in Table 1. The powders were sampled following ASTM B215-15 scoop method and characterised based on the techniques and standards shown in Table 2.

Table 1: IN625 powder specifications

Powder	Specification	Remarks
A	15 – 45 µm	Typical size range for L-PBF
B	0 – 45 µm	Increase in amount of fine particles / wider particle size range
C	0 – 32 µm	Decrease in particle mean size

Table 2: Powder characterisation techniques and standards

Powder Characterisation	Techniques / Equipment	Reference
Particle Size Distribution (PSD)	Static Image Analysis (Morphologi G3)	ISO 13322-1:2014
True Density	Helium Pycnometry	ASTM B923-16
Apparent Density	Hall Flowmeter Funnel	ASTM B212-17
	Carney Funnel	ASTM B417-13
Tap Density	Tap Density	ASTM B527-15
Flowability	Hall Flow Rate	ASTM B213-17
	Carney Flow Rate	ASTM B964-16

Layering assessment and coupon fabrication were performed for each powder in virgin condition at a layer thickness of 40µm. All coupons were processed using standard OEM process parameters and post-processing procedures i.e. heat treatment and EDM wire-cutting for part removal. Each build consisted of coupons with internal channels of 5mm diameter printed vertically and horizontally, as well as density cubes, tensile bars and powder capsules. The build layout is shown in Figure 2.

(a) Build design **(b) As-built parts**

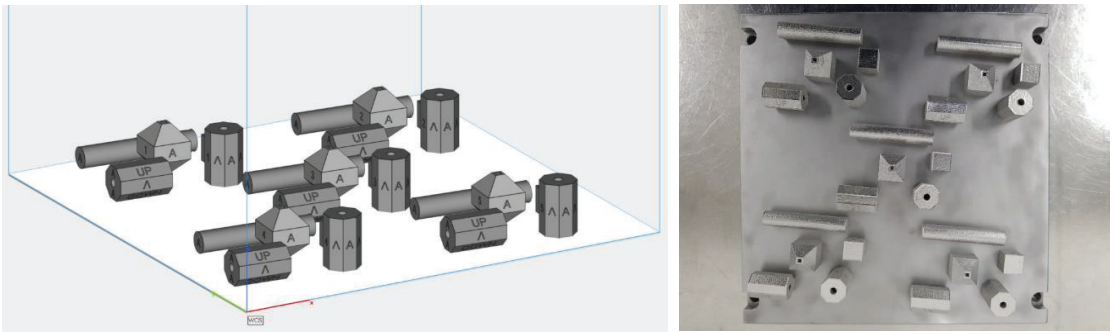

Figure 2: Build layout of coupons

The powder capsules were used to collect the powder in the build chamber during the fabrication process. The powder layer density for each build was determined using the following equation:

$$Powder\ Layer\ Density = \frac{Mass\ of\ Powder\ Collected}{Internal\ Volume\ of\ Capsule} \quad (3)$$

The density cubes were used for density analysis and hardness testing while the tensile bars were machined into standard specimen size for tensile testing. The parts were characterised based on the techniques and standards as shown in Table 3.

Table 3: Part characterisation techniques and standards

Part Characterisation	**Techniques / Equipment**	**Reference**
Density	Archimedes Principle	ASTM B311-17
Hardness	Micro Vickers Hardness Testing	ASTM E384-17
Tensile Strength	Tensile Testing	ASTM E8-16a

The coupons with vertical and horizontal internal channels were sectioned using EDM wire-cutting for inspection of the internal surfaces. Surface quality was characterised with areal surface texture parameters i.e. S_a and S_z measured using the *Taylor Hobson Talysurf CCI-HD*, a non-contact 3D optical profiler. Compared to conventional line measurements that provide 2D roughness profiles, areal analysis provides 3D surface topography information which can be more comprehensive and useful for characterising highly irregular AM surfaces. A 20X magnification lens was used to give a spot area of 0.83mm x 0.83mm for each measurement. The features measured are shown in Figure 3. Five coupons were fabricated for each feature and the measurements were taken at three locations for each coupon. An overall average was used for analysis.

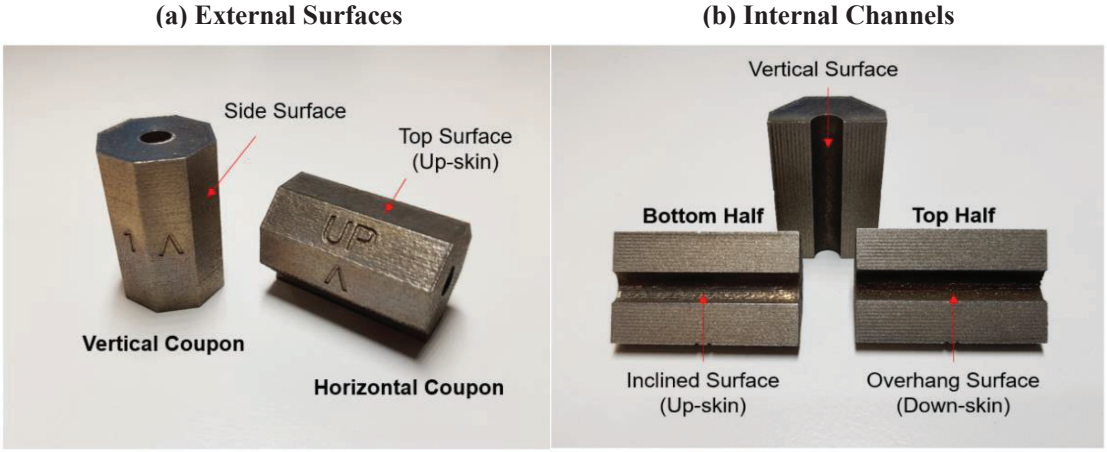

Figure 3: Features measured for surface quality evaluation

Results and Discussion

Powder Characterisation

The static image analysis was done using the *Malvern Morphologi G3*, which captures the 2D image of the particle and converts it into a circle of equivalent area reported as Circle Equivalent (CE) diameter. It provides a number-based distribution (n) which is more sensitive to smaller particles and is more effective in characterising metal powders in L-PBF containing relatively fine particles. The results are shown in Table 4. Span is a measure of distribution width defined as:

$$Span = \frac{D90-D10}{D50} \quad (4)$$

A higher span represents a wider particle size distribution. Results showed that Powder C had the lowest particle mean size while Powder B had the highest span, suggesting a wider particle size range due to the presence of both small and large particles.

Table 4: PSD results from number-based distribution

Powder	A	B	C
D[n,0.1] (µm)	19.70	15.21	13.25
D[n,0.5] (µm)	27.42	25.57	23.01
D[n,0.9] (µm)	40.74	36.59	31.76
Mean (µm)	29.27	26.14	23.49
Span (n)	0.77	0.84	0.80

True, apparent and tap densities were measured using samples from the feedstock powder before each build. The powder layer density was calculated from equation (3) using the powder collected in the capsules after each build. True density, which is the absolute density of the powder material IN625, was measured to be 8.55g/cm^3 using helium pycnometry. This value was considered as 100% density for the computation of relative densities as shown in Table 5.

Table 5: Density (g/cm³) and relative density (%) for different powders

Powder	True Density (g/cm³)	Apparent Density (g/cm³)	Tap Density (g/cm³)	Powder Layer Density (g/cm³)
A	8.55 ± 0.01 (100%)	3.89 ± 0.02 (45.50%)	4.79 ± 0.02 (56.02%)	4.47 ± 0.02 (52.28%)
B	8.55 ± 0.01 (100%)	4.02 ± 0.02 (46.90%)	5.01 ± 0.04 (58.60%)	4.54 ± 0.01 (53.10%)
C	8.55 ± 0.00 (100%)	3.95 ± 0.02 (46.20%)	4.96 ± 0.02 (58.01%)	4.51 ± 0.01 (52.75%)

Apparent density provides an indication to a powder's natural packing ability upon free flowing through a nozzle while tap density measures the powder's ability to re-arrange itself upon mechanical tapping. However, it may not be accurate representations of powder behaviour in L-PBF where the powder is deposited on the build platform by a coater blade layer by layer. The powder layer density measurement would provide a better estimate of powder density, hence would be used to calculate the effective layer thickness for each powder.

From the results, Powder B had the highest apparent and tap densities followed by C and A. Powder layer density displayed a similar trend with values in between apparent and tap density. The difference in powder densities could be correlated to the particle size range where Powder B was shown to have the highest span followed by C and A. The higher the span, the higher the powder densities. This is because with a wider particle size range, small particles can fill into the voids between large particles allowing them to be packed closer to each other.

Powder flowability is influenced by inter-particle interactions such as frictional forces, mechanical interlocking, and adhesion due to moisture ingress. These factors are in turn affected by PSD, morphology, and surface chemistry of the powder. Powder flowability is conventionally represented by Hall and Carney flow rates, which measures the time taken for a fix mass of powder to flow through a calibrated funnel. The longer the time taken, the poorer the flowability. Another measure of flowability is the Hausner Ratio (HR), a parameter correlating powder density and flowability. The higher the HR, the poorer the flowability. The Hausner Ratio is the ratio of tap density to apparent density as shown in the following equation:

$$Hausner\ Ratio = \frac{Tap\ Density}{Apparent\ Density} \quad (5)$$

The Hall and Carney flow rates are shown in Table 6 and the mean values were compared with the Hausner Ratio for each powder as shown in Figure 4.

Table 6: Hall and Carney flow rates for different powders

Hall Flow Rate - FR_H (s/50g)					
Powder	**Run 1**	**Run 2**	**Run 3**	**Mean**	**St Dev**
A	18.18*	17.30*	17.21*	17.56	0.54
B	No flow	No flow	No flow	-	-
C	No flow	No flow	No flow	-	-
Carney Flow Rate – FR_c (s/150g)					
Powder	**Run 1**	**Run 2**	**Run 3**	**Mean**	**St Dev**
A	11.24	11.50*	11.32	11.35	0.13
B	11.74	12.49*	12.34*	12.19	0.40
C	14.53*	13.29*	13.12*	13.65	0.50
* Flow after tapping					

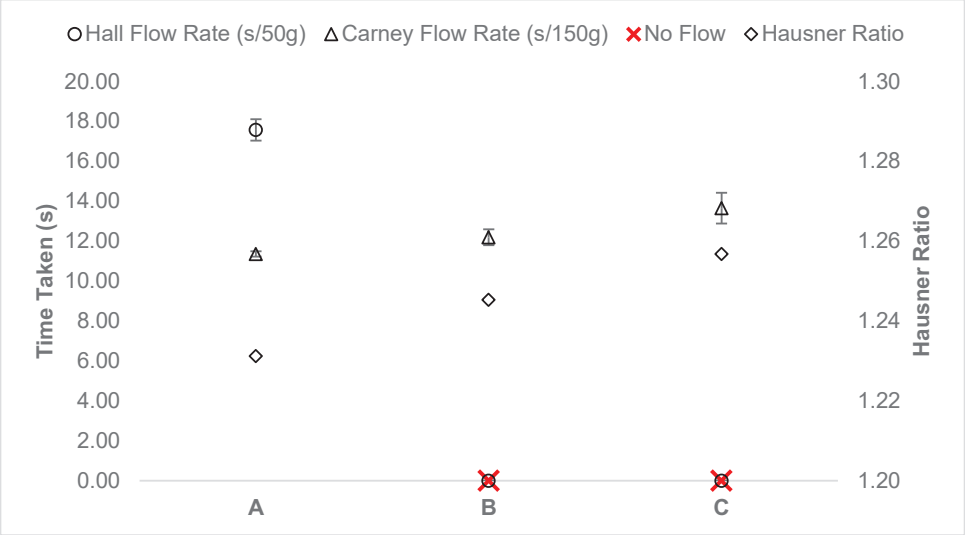

Figure 4: Results for flowability and Hausner Ratio

Powder A flowed through the Hall flow funnel but required tapping, but no flows were recorded for Powder B and C even after tapping, suggesting poorer flowability compared to Powder A. All three powders flowed through the Carney flow funnel and the results confirmed that Powder A had the highest flow rate, followed by B and C. The poor flowability of Powder B and C could be due to the presence of small particles resulting in a higher surface area per unit mass for frictional forces to act between the particles and increasing inter-particle cohesion. In general, the smaller the particle mean size, the poorer the flowability. The Hausner Ratio results followed a similar trend and further supports the observation.

Layering Assessment

Prior to actual part fabrication, layering assessment was conducted to evaluate the processability of each powder in virgin condition. The steps involved depositing powder on the build platform for the first 10 layers at a layer thickness of 40µm and photographing an image with a camera for each layer. The quality of powder bed was inspected by visual means based on the following guidelines:

- Even distribution of powder covering the entire surface of the build area
- Smooth and flat surface of powder layer, surface is not wavy or undulating
- No observable irregularities such as scratch lines, holes, and agglomerated particles

For all 10 layers of deposition for Powder A and B as no irregularities were detected. However, some scratch lines were seen in the first three layers for Powder C, stretching across the powder bed in the coating direction as shown in Figure 5. The scratch lines did not appear after the third layer of deposition and would not affect the fabrication of coupons or final part properties since it lies within the region of material that would be removed during wire-cutting for part removal. Scratch lines are typically formed when particles agglomerate and adhere to the edge of the coater blade and are dragged across the powder bed. This usually occurs in powders that exhibit high cohesiveness due to the presence of fine particles or irregularly shaped particles. In the case of Powder C, the fine particles with high cohesiveness might be the cause for scratch lines in the first few layers of powder deposition.

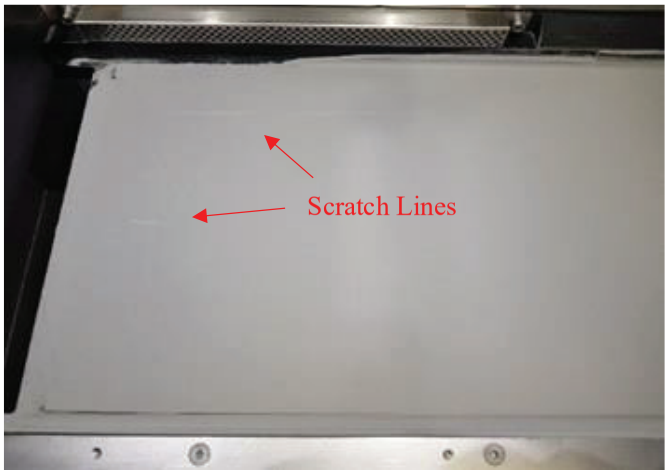

Figure 5: Scratch lines in third layer deposition of Powder C

Part Characterisation

Part density was measured using Archimedes' principle for the cubes fabricated by each powder. Relative density was calculated based on the true density of the powder measured at 8.55 g/cm³ (100%). Micro Vickers hardness test was also performed on the XY and XZ planes of the cubes. Table 7 shows the density and hardness testing results. The change in PSD and powder densities showed no clear correlation to the final part density and hardness values.

Table 7: Density and hardness of coupons fabricated using different powders

Powder	Part Density (g/cm³)	Relative Density (%)	HV/1 - XY	HV/1 - XZ
A	8.515 ± 0.003	99.59 ± 0.04	290.4 ± 3.1	294.3 ± 5.0
B	8.522 ± 0.004	99.67 ± 0.04	290.6 ± 2.6	287.2 ± 3.7
C	8.518 ± 0.003	99.63 ± 0.03	295.3 ± 5.1	285.6 ± 5.3

Tensile testing was conducted with horizontal tensile bars that were heat-treated and machined to a standard specimen size. The results for Ultimate Tensile Strength (UTS), 0.2% Yield Strength (0.2%YS) and Failure Strain are shown in Table 8. Based on the results, there was negligible difference in tensile properties between coupons fabricated by the three powders. The change in PSD did not show any significant effect on the static mechanical properties of the final parts.

Table 8: Tensile test results for horizontal tensile specimens

Powder	UTS (MPa)	0.2%YS (MPa)	Failure Strain (%)
A	950 ± 5	647 ± 4	28.7 ± 1.5
B	953 ± 12	650 ± 9	28.2 ± 0.5
C	936 ± 8	637 ± 9	28.1 ± 0.9

Effective Layer Thickness

All coupons were fabricated using a theoretical layer thickness (t_0) of 40µm. The effective layer thickness (t_{eff}) was calculated based on the powder layer density and part density of each build using equations (1) and (2). The t_{eff} for t_0 = 40µm and t_0 = 20µm were determined and compared with the D_{90} of each powder as shown in Figure 6.

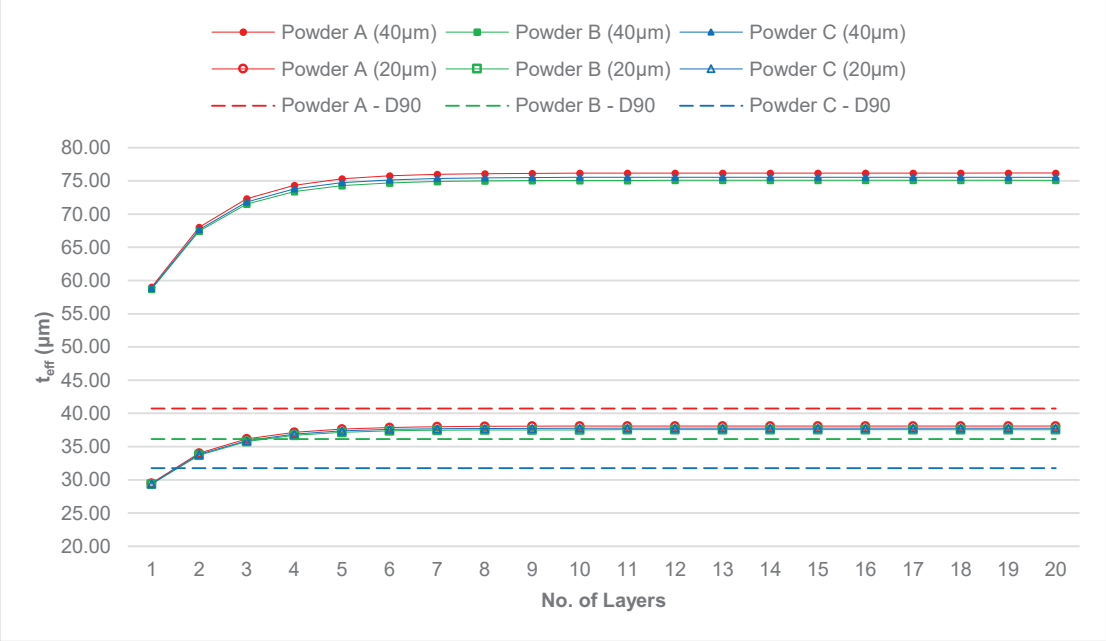

Figure 6: Effective layer thickness (t_{eff}) over 20 layers

To determine the effects of PSD on surface finish, the effective layer thickness has to be considered in relation to the particle size. For a theoretical layer thickness of $t_0 = 40\mu m$, the effective layer thickness for all powders reached above 76µm, which was much greater than the size of the powders ($t_{eff} > D_{90}$). Large particles could be deposited in the powder layer so surface roughness would be attributed to the size and quantity of the large particles present and the effect of small particles would become less significant. Since the main difference between Powder A (15 - 45µm) and B (0 - 45µm) was in the amount of small particles present, the improvement in surface finish of parts produced by Powder B compared to A might not be obvious. However, Powder C (0 - 32µm) would be expected to produce parts with a better surface finish as it has a smaller D_{90} and mean size compared to A and B.

The influence of PSD on surface finish might change for a lower effective layer thickness. For example, if the theoretical layer thickness is $t_0 = 20\mu m$, the effective layer thickness achieved will only be about 38µm, which is below the D_{90} of Powder A ($t_{eff} < D_{90}$) but above that of B and C. The same explanation cannot be used for Powder A as particles that are larger than t_{eff} will not be deposited in the powder layer. In this case, the effect of large particles present will be less significant in increasing surface roughness.

Surface Quality

For external surfaces, the results for top and side surface roughness in terms of S_a and S_z are shown in Figure 7. Results showed that top surfaces exhibit better surface finish than side surfaces. While Powder C produced the lowest average S_a and S_z values for both surfaces, the differences between the results for all three powders were marginal.

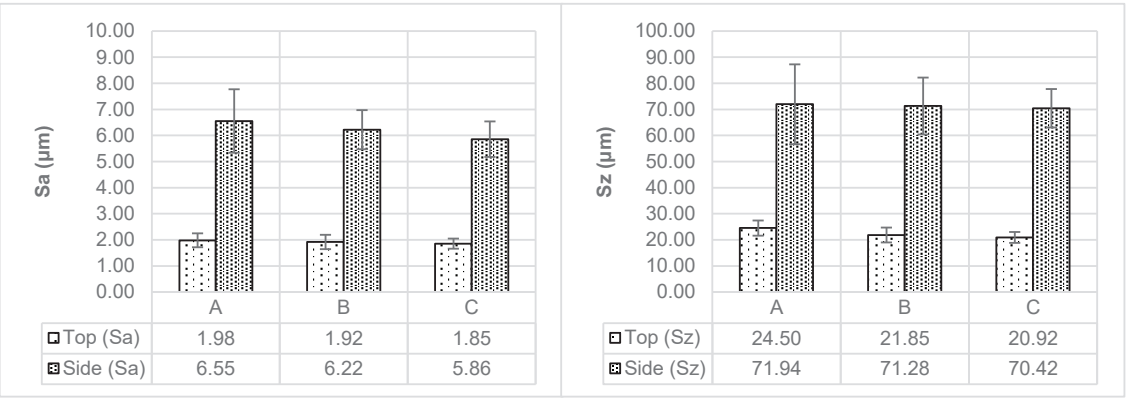

Figure 7: Surface roughness results for external surfaces

Figure 8 shows the top and side surface topographies obtained for each powder. Top surfaces roughness was mainly caused by surface undulation formed from the laser scan tracks and the effect of PSD was not obvious. In contrast, side surface roughness was attributed to the presence of partially sintered particles adhering to the surfaces. Naturally, the smaller the size of these particles, the lower the roughness values.

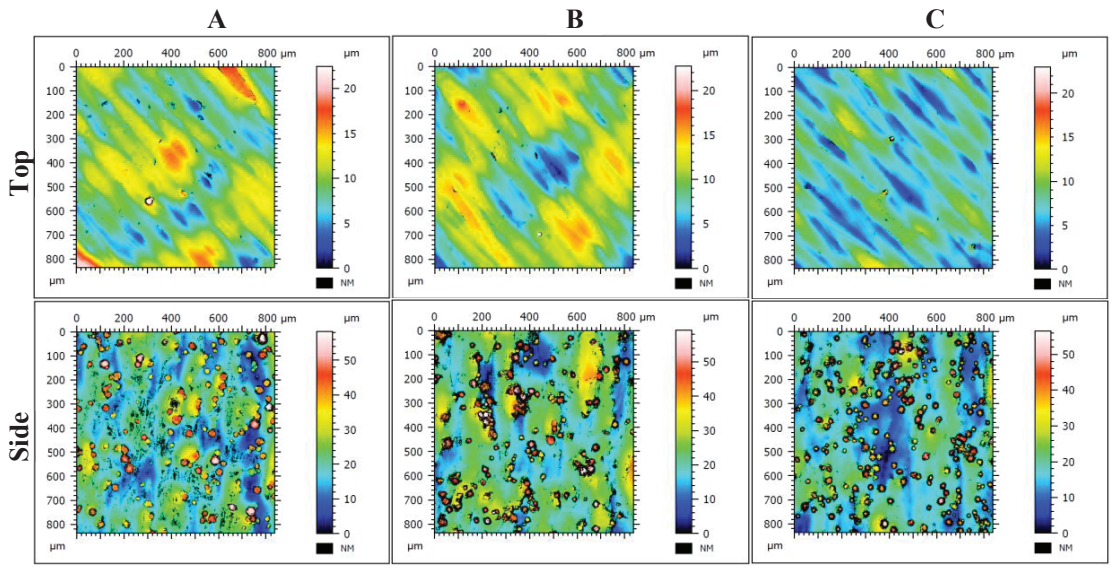

Figure 8: Surface topography for top and side surfaces

For the internal channels, vertical surface refers to the internal surface of the vertical channel while inclined and overhang surfaces refer to the up-skin and down-skin of the horizontal channel. The surface roughness results in terms of S_a and S_z are shown Figure 9. Results showed that overhang surfaces exhibit the poorest surface finish with the highest S_a and S_z values. Inclined surfaces had lower S_a values but higher S_z values compared to vertical surfaces. Similar to the observations for external surfaces, Powder C produced the lowest S_a and S_z values for all internal surfaces but the improvement in surface finish was only to a small extent.

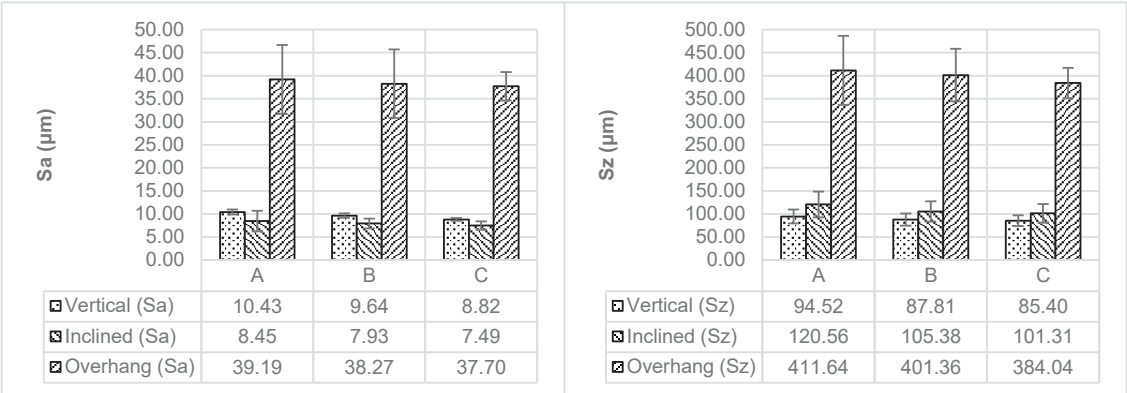

Figure 9: Surface roughness results for internal channels

Figure 10 shows the vertical, inclined and overhang surface topographies obtained for each powder. Partially sintered particles were seen on all surfaces but in different sizes and quantities for different surfaces.

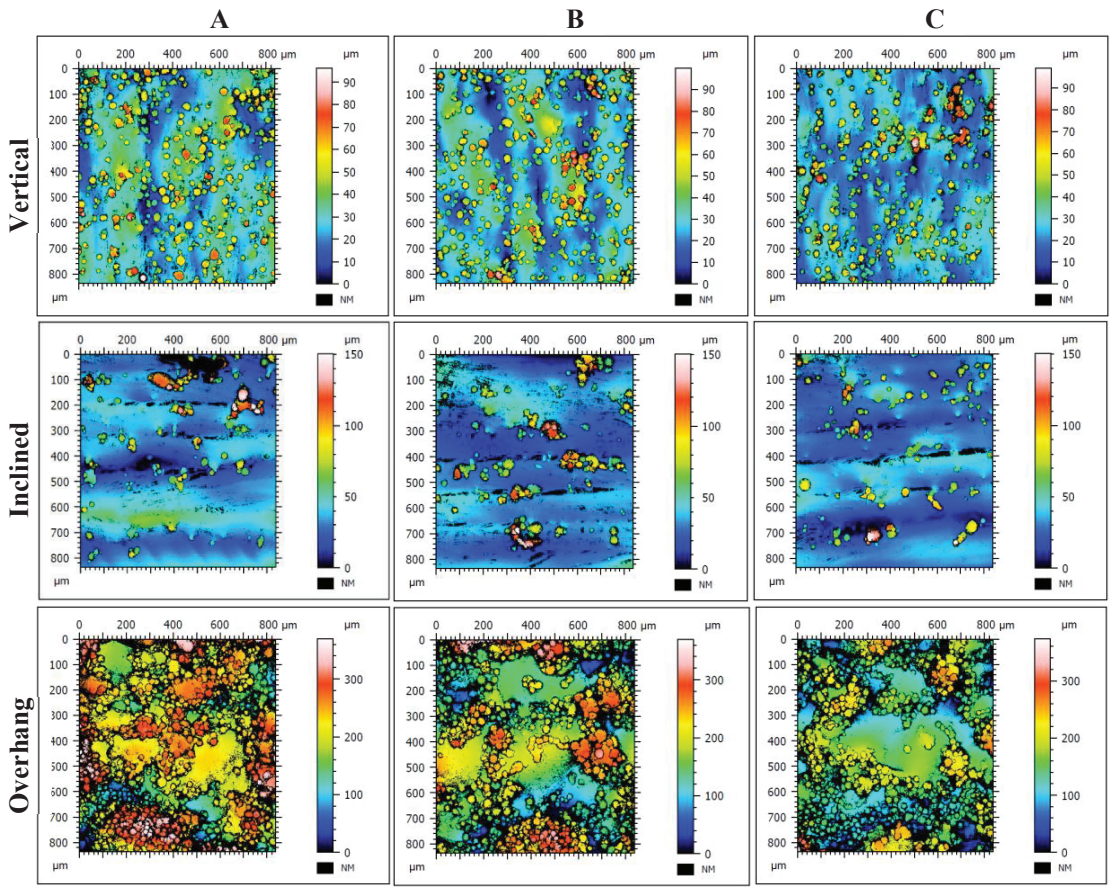

Figure 10: Surface topography for vertical, inclined and overhang surfaces

Vertical surfaces showed similar characteristics to side surfaces in terms of the amount of partially sintered particles. Inclined surfaces seemed to have a lower amount of partially sintered particles but tend to be larger in size and irregularly shaped. This might be the reason for the lower S_a but higher S_z values compared to the vertical surfaces. Surface roughness was also influenced by the staircase effect evident from the dark valleys shown in the surface topography. The staircase effect is unique to inclined surfaces where the higher the layer thickness, the higher the surface roughness. Overhang surfaces had the highest amount of partially sintered particles causing highly irregular surface topographies. This is because during the fabrication, the overhang surfaces were in direct contact with the powder bed and not supported by scanned bulk layers or support structures.

Conclusion

To study the effects of PSD on surface finish of SLM parts, IN625 powder of three different PSDs were characterised and processed using 40µm layer thickness, standard processing and post processing parameters. Powder B had the widest particle size range, resulting in the highest powder layer density. Powder C had the smallest particle mean size, resulting in high cohesiveness and poor flowability, which was also evident from the irregularities i.e. scratch lines seen in the first few layers of powder deposition. The change in

PSD showed no significant effect on the final part density, hardness and static mechanical properties.

The t_{eff} for t_0 = 40 μm was shown to be greater than the particle size of all powders, suggesting that surface roughness would be attributed to the size and quantity of the large particles present and the effect of small particles would become less significant. Results showed that Powder C produced surfaces with the lowest average roughness values, suggesting that a lower particle mean size led to small improvements in surface finish for both external and internal surfaces. From the surface topographies obtained, it can be seen that the roughness of internal surfaces was mainly attributed to the size and quantities of partially sintered particles. This means that particle mean size will have a direct influence on surface roughness as the larger the size of the partially sintered particles, the higher the roughness values. t_{eff} also plays a part as it determines the amount of large particles that can be deposited in the powder layer. In general, a smaller particle mean size and wider particle size range would be preferred for better surface finish, but a powder that is too fine may result in poor flowability affecting its processability in terms of layering and powder bed quality.

Powder behaviour can differ across AM platforms with different layering mechanism. This study was conducted using a stiff coater blade made of steel. It can be extended to evaluate the effects of powder characteristics on surface finish using coater blades of different material, geometry and stiffness, or with a roller coating mechanism. Surface finish can also be affected by the chemical properties of powder. Further research can include analysis on surface chemistry, moisture content, oxide layer formation, or melt pool characteristics and their effects on surface finish.

References

[1] M. L. Vlasea, B. Lane, F. Lopez, S. Mekhontsev, A. Donmez, 26th Annu. Int. Solid Free. Fabr. Symp. 2015, 527.

[2] N. Guo and M. C. Leu, "Additive manufacturing: Technology, applications and research needs," Front. Mech. Eng., 2013, vol. 8, no. 3, pp. 215–243.

[3] Mumtaz, K. and Hopkinson, N., Top surface and side roughness of Inconel 625 parts processed using selective laser melting. *Rapid Prototyping Journal*, 2009, *15*(2), 96–103.

[4] D.L. Bourell, H.L. Marcus, J.W. Barlow, and J.J. Beaman, *Int. J. Powder Metall.*, 1992, vol. 28 (4), pp. 369-81.

[5] Rehme, O. *Cellular Design for Laser Freeform Fabrication*, 2010

[6] Elsen, M. Van, Al-Bender, F., and Kruth, J.-P., Application of dimensional analysis to selective laser melting. *Rapid Prototyping Journal*, 2008, *14*(1), 15–22.

[7] Pupo, Y., Monroy, K. P., and Ciurana, J., Influence of process parameters on surface quality of CoCrMo produced by selective laser melting. *International Journal of Advanced Manufacturing Technology*, 2015, 985–995.

[8] D.E. Bunnell, S. Das, D.L. Bourell, J.B. Beaman, and H.L. Marcus, *Proc. Solid Freeform Fabrication Symp*., 1995, The University of Texas at Austin, Austin, TX, pp. 440-47.

[9] Kruth, J.-P., Mercelis, P., Van Vaerenbergh, J., Froyen, L., Rombouts, M., Binding mechanisms in selective laser sintering and selective laser melting. Rapid Prototyping Journal, 2005, 11 (1), 26–36.

[10] Kruth, J.-P., Levy, G., Klocke, F., Childs, T.H.C., Consolidation phenomena in laser and powder-bed based layered manufacturing. CIRP Annals – Manufacturing Technology, 2007, 56 (2), 730–759.

[11] Liu, Bochuan & Wildman, Ricky & Tuck, Christopher & Ashcroft, Ian & Hague, Richard, *Investigation the effect of particle size distribution on processing parameters optimisation in selective laser melting process*. 22nd Annual International Solid Freeform Fabrication Symposium - An Additive Manufacturing Conference, SFF 2011.

[12] A.B. Spierings, N. Herres, G. Levy, *Influence of the particle size distribution on surface quality and mechanical properties in AM steel parts*. Rapid Prototyping Journal, 2011, Vol. 17 Issue: 3, pp.195-202

[13] A.B. Spierings, G. Levy, *Comparison of density of stainless steel 316L parts produced with Selective Laser Melting using different powder grades*. 20th Annual International Solid Freeform Fabrication Symposium, SFF 2009.